Sigma phase precipitation modelling in a UNS S32760 superduplex stainless steel

P. Ferro, F. Bonollo, G. Timelli

Sigma phase precipitation is known to have detrimental effects on mechanical and corrosion properties in stainless steels. Accordingly, heat treatments and welding must be performed carefully. For this reason, computer models which predict the evolution of secondary phases with the temperature are very useful for a good planning of industrial heat treatments or welding. A semiempirical model, based on the pioneer work of Wilson and Nilsson, describing the microstructural evolution of UNS S32760 superduplex stainless steels was developed. The computer model, based on the modified Johnson–Mehl–Avrami-Kolmorgorov (JMAK) type of equation, uses information from isothermal experiments of sigma-phase transformation and predicts the transformation kinetics during a cooling process. A good agreement was found between the predicted CCT-diagram and the experimental tests.

Keywords:
Duplex Stainless Steel, UNS S32760, Heat Treatment, Sigma Phase, model, TTT, CCT, additivity rule

1. INTRODUCTION

Duplex and Superduplex Stainless Steels (SDSS) are two-phases alloys consisting of approximately equal proportions of ferrite (δ) and austenite (γ) phases. This balanced microstructure offers a combination of high toughness, good weldability, satisfactory corrosion resistance and high strength [1]. The main difference between Duplex and Super Duplex grade is the content of chromium and nitrogen which is higher in the SDSS. In particular, PREN (Pitting Resistance Equivalent Number) [1] values for SDSS are greater than 40, which indicates a higher pitting corrosion resistance as well as a longer life span if compared to standard Duplex Stainless Steel.

The knowledge of microstructural evolution of such kind of steels, as the result of their thermal history, is a fundamental issue to achieve the expected mechanical behaviour and corrosion resistance. The time-temperature history, deriving for instance from industrial heat treatments or welding processes [2,3], may lead to precipitation of various compounds, such as chromium carbides and nitrides, and some other intermetallic phases like the σ one. The formation of such compounds leads to loss in both corrosion resistance and fracture toughness [1-6].

In particular, sigma phase is a Cr- and Mo-rich intermetallic phase which can arise after relatively long holding times at temperatures ranging from 650 to 950 °C as well as after cooling from high temperatures or in the heat-affected zone produced by welding. The precipitation rate of σ phase is maximum for isothermal ageing carried out at temperature around 850°C. The higher the ageing temperature the bigger the sigma phase grains [7,8]. In the case of duplex stainless steels, precipitation can be complete in a few hours and consume all the ferrite of the microstructure [9]. In this case precipitation can be represented by an euctectoid-type reaction: $\alpha \rightarrow \gamma* + \sigma$, where γ* is a chromium and molybdenum depleted austenite if compared to a non-transformed austenite. Precipitation starts at the α/γ interface and moves into ferrite grains until ferrite is practically exhausted [10]. Up to 800 °C the euctectoid morphology is nearly lamellar resulting from sigma and austenite cooperative growth whereas around 900 °C the sigma phase precipitates in a massive morphology leading to a microstructure called divorced eutectoid [10]. Conversely, the nucleation of the sigma phase along ferrite/ferrite grain boundaries suggests that the direct reaction $\alpha \rightarrow \sigma$ can also occur. The new austenite (γ*) is essentially a Fe-Ni alloy which is nearly molybdenum-free and whose chromium content is low.

Sigma phase precipitation dramatically decreases the toughness of DSS (Duplex Stainless Steels) [11-13]. Already about 1% of sigma phase implies an impact value drop of about 50% relative to initial conditions (solution annealed and quenched) [14]. Good toughness properties are achieved by applying proper solution temperatures and cooling rates [15-16]. Moreover sigma phase might deteriorate corrosion properties since Mo and Cr accumulate in this phase.

The precipitation of sigma phase is a nucleation and growth process whose kinetic is controlled both by thermodynamic driving forces and diffusion. Sieurin et al. [7] have modelled the sigma precipitation in DSS 2205 during isothermal heat treatments and continuous cooling from high temperatures assuming that Mo controls the transformation in the ferrite matrix and also that only equilibrium contents of Mo in the ferrite and sigma phase are needed for calculations. Thermo-Calc [17] was utilised to obtain the compositions and diffusion coefficients as a function of temperature. It is worth-mentioning that a very fast nucleation rate was calculated so that sigma precipitation is controlled by the growth. In another paper, Li et al. [18] developed a model for sigma phase isothermal precipitation starting from the Avrami equation and thermodynamic calculations by Thermo-Calc. Specific parameters such as wetting angle, number of potential sites for nucleation and the Avrami exponent, were evaluated mainly through matching the experimental results for transformation in SAF 2205 and SAF 2507. Once again, in that work, it was verified that nucleation is so easy that conditions of nucleant site saturation were applied in many of the cases considered.

About the semi-empirical models, Kim et al. [19] have used the additivity rule (suggested by Scheil [20]) to calculate the Continuous Cooling Transformation (CCT) diagrams in cast duplex

P. Ferro, F. Bonollo, G. Timelli
DTG University of Padova, Str. S. Nicola, 3 I-36100 Vicenza – Italy

stainless steels. The mathematical expression of the additivity rule is as follows:

$$\int_0^{t_X} \frac{dt}{\tau_X(T)} = 1 \quad (1)$$

where $\tau_X(T)$ is the time used for the transformed volume fraction to reach X under an isothermal temperature T, and t_X the time to reach X under continuous cooling. The additivity rule can also be described as a transformation continuing at a new temperature as though the earlier transformation had occurred at the new temperature. At any temperature, the transformation rate is then only a function of previously-transformed fraction and the transformation temperature.

The additivity rule assumes that all nucleation takes place at the early stage of the reaction. This assumption is generally made in situations involving continuous cooling where heterogeneous nucleation occurs and is often referred to as site saturation. Nucleation effects are negligible under this condition so that growth is the predominate mechanism for a reaction [19]. In that work, Kim et al. [19] considered the Avrami exponent taken from experimentally determined Time-Temperature Transformation (TTT) diagrams as a function of temperature and calculated the corresponding CCT diagrams through a modified Avrami equation. However, even if experimental and predicted results were in good agreement, some theoretical doubts about the applicability of the additivity rule in such conditions arise. As a matter of fact, in ref. [21], Lusk and Jou demonstrated that if the Avrami exponent is a function of temperature then the rule of additivity cannot be applied even thought the kinetics is rate independent. In their work, Wilson and Nilsson [22] developed a computer semi-empirical model for sigma precipitation in DSS under continuous cooling. The cooling curve was approximated by a series of small isothermal steps. It was assumed in these calculations that the evolution of intermetallic phase could be described by an Avrami equation such as $V/V_{eq}(T) = 1-\exp(b(T)t^{n(T)})$, where V is the volume fraction of intermetallic phase, V_{eq} is the corresponding equilibrium volume fraction at temperature T, b(T) and n(T) are experimentally determined and optimized from previous Avrami equation using isothermal data. The same model was used for the study of σ-phase formation in 29Cr-6Ni-2Mo-0.38N Superduplex Stainless Steel [23]. It is interesting to note that in that work it was found that Thermo-Calc fails to faithfully predict the dissolution temperature of sigma phase. The same conclusion was also achieved in the work of Elmer et al. [24].

In the present work, a semiempirical model, based on the work of Wilson and Nilsson [22], describing the microstructural evolution of UNS S32760 superduplex stainless steels was developed. This model uses data from isothermal experiments for its calibration and, compared to the Wilson and Nilsson work, is based on a modified Johnson–Mehl–Avrami-Kolmorgorov (JMAK) type of equation.

2. CALCULATION OF TIME-TEMPERATURE TRANSFORMATIONS (TTT) DIAGRAMS

The proposed model is based on the modified JMAK transformation kinetic equation proposed by Lee et al. [25] which takes the form:

$$y = 1 - \left[\frac{1}{1+c(bt)^c}\right]^n \quad \text{with } b, c > 0 \quad (2)$$

where:

- $y = V/V_{max}$ is the fraction of initial phase transformed at time t(V) normalized by the maximum amount of phase formed at the end of transformation (V_{max});
- c is the so-called impingement exponent;
- b is a constant which takes into accounts the effects associated with nucleation and growth and usually empirically evaluated for each temperature.

The rearranged form of equation (2) was used for optimizing the b and n parameters from several measurements by a least square method:

$$\ln\left|\frac{(1-y_i)^{-c}-1}{c}\right| = n\ln t + n\ln b \quad (3)$$

In equation (2) c was considered constant with the temperature while V_{max} has to be estimated preferably by long-time annealing experiments. Thus, by using equation (4) it is possible to plot the level curves in the TTT-diagram.

$$\tau_i = \frac{1}{b_i}\left|\frac{(1-y_i)^{-c}-1}{c}\right|^{\frac{1}{n}} \quad (4)$$

In equation (4) τ_i is the isothermal transformation time for the level of transformation V_i. For intermediate temperature not included in the experiments, the times τ_i are logarithmically interpolated. This interpolation corresponds to a straight line between the points in the TTT-diagram.

3. CALCULATION OF CONTINUOUS-COOLING TRANSFORMATIONS (CCT) DIAGRAMS

Following the Wilson and Nilsson approach [22], by using equation (3), two level curves, chosen by the user, are stored (i=1,2). Each cooling curve used for determining the CCT-diagram is then approximated with a stair-case curve using a temperature decrement of 1 °C and a corresponding time increment Δt (Fig. 1).

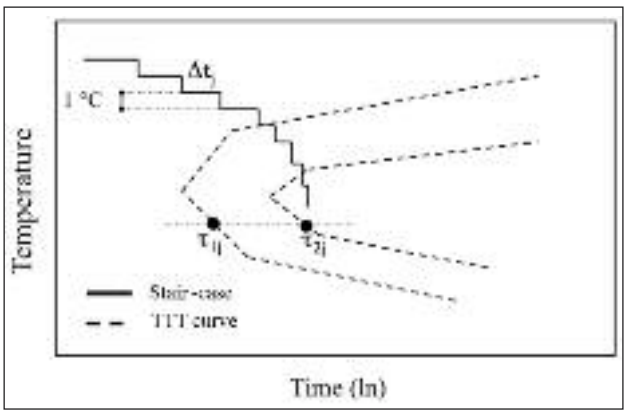

FIG. 1 ***Schematic description of the main parameters involved in the model.***

Descrizione schematica dei principali parametri del modello.

For each temperature step (j), the n_j and b_j parameters are determined by using equations (5) and (6)

$$n_j = \frac{\ln\left[\frac{(1-y_{2j})^{-c}-1}{(1-y_{1j})^{-c}-1}\right]}{\ln\left(\frac{\tau_{2j}}{\tau_{1j}}\right)} \quad (5)$$

$$b_j = \frac{1}{\tau_{1j}}\left|\frac{(1-y_{1j})^{-c}-1}{c}\right|^{\frac{1}{n_j}} \quad (6)$$

and the contribution of the transformation at the step j-1 is thus taken into account by a fictitious time according to equation (7) (V_{j-1}=0 and t'_j=0 for the first step):

$$t_j = \frac{1}{b_i}\left[\frac{(1-Y_{j-1})^{-c}-1}{c}\right]^{\frac{1}{n}} \quad (7)$$

Finally, the transformed fraction y_j after the step j is calculated by using eq. (8) where Δt_j is the stair-case time increment:

$$Y_j = Y_{max}\left[1-\left(\frac{1}{1+c(b_i(t'_j+\Delta t_j))^n}\right)^{1/c}\right] \quad (8)$$

The volume fraction transformed is stored for each temperature down to room temperature and is used for the CCT-diagram plotting.

4. UNS S32760 SUPERDUPLEX STAINLESS EXPERIMENTAL CHARACTERIZATION

The analysed material (UNS S32760) was available in the solution and water quenched state. The chemical composition is given in Table 1.

The as-received material presented a good balance of ferrite-austenite phases (55/45), and no secondary precipitates. Beraha's tint etch (20 ml HCl and 80 mL H_20, 1g $K_2S_2O_5$) was used to produce contrast between the ferrite and austenite. The volume fraction of the two phases has been measured in 10 fields by Image Analysis. Cylindrical specimens (diameter: 20 mm; height: 20 mm) have been used for heat treatment experiments. In order to promote phase precipitation, they have been heat-treated in furnace under different conditions. Based on literature overview, temperatures for isothermal heat treatments have been chosen around 900 °C. In particular, treatments at temperatures of 800, 900, 950 and 1000 °C, for time intervals of 1, 3, 10, 30, 180 and 420 min, have been performed.

During the treatments, the temperature has been measured by k-type thermocouples applied into the core and near the surface of the specimens.

Some anisothermal heat treatments have been also carried out, in order to study the continuous cooling kinetics of sigma precipitation. Specimens have been heated up to 1050°C and then cooled at different cooling rates (4, 0.19, 0.044 °C/s) (air cooling, furnace cooling with door opened and door closed [26]).

σ phase was analysed by optical microscopy, after electrolytic etching (50g KOH, 100 ml H_2O); LEICA QWIN Image Analysis code has been adopted to determine the sigma phase content. Fig. 2 shows some micrographs referred to isothermally heat treated specimens. The average amount of sigma phase and the related standard deviations have been calculated working on 16 fields, with the results summarized in Table 2.

The σ-phase amounts obtained by anisothermal heat treatments have been collected in Table 3, while the corresponding microstructure are shown in Fig. 3.

The plot of ln(-ln((1 − y)) = f(ln t) for the sigma-phase precipitation in the UNS S32760 SDSS used in this work is shown in Fig. 4. It is clearly seen that the experimental data points deviate from a straight line. Consequently, the precipitation kinetic of the sigma-phase in the present SDSS does not agree with the classical Avrami model (Eq. (9)). This model was recently modified by Lee et al. [25] in order to take into account the complex competing effects which may occur during precipitation of sigma-phase: the untransformed term (1−y) in Eq. (9) is thus now considered to contain an impingement factor, used to correct some effects such as a depletion of the solute content in the

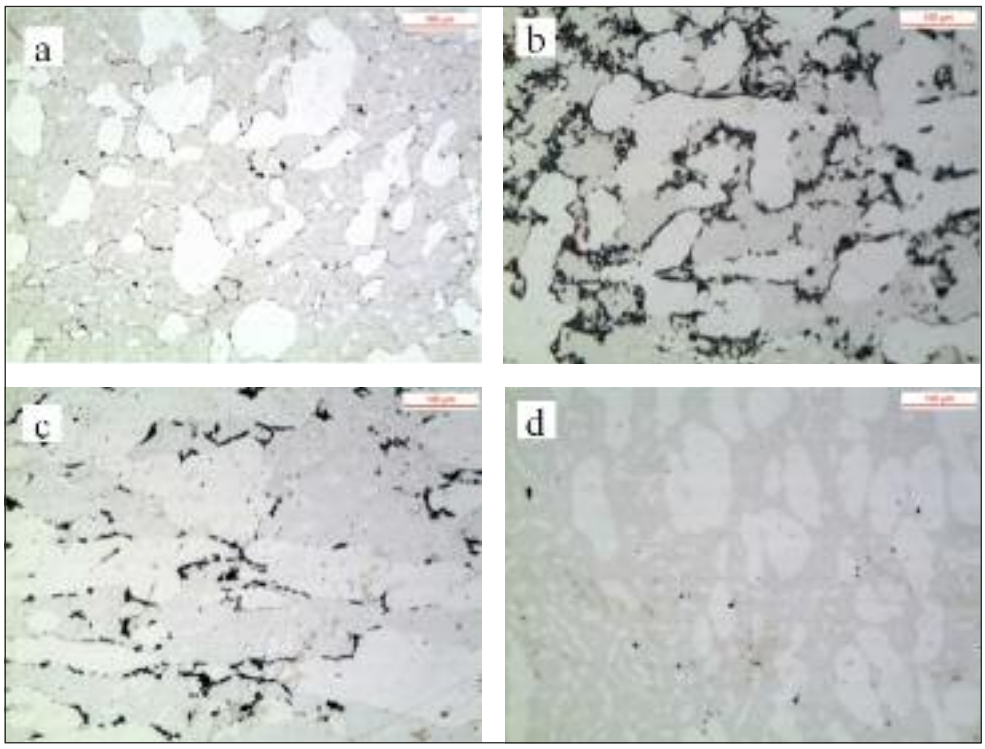

FIG. 2
Microstructure of the heat-treated material a) 800°C, b) 900°C, c) 950°C, d) 1000 °C Black phase: σ-phase (τ=3 min).
Fig. 2: Microstruttura del materiale dopo trattamento a temperatura costante a) 800 °C, b) 900 °C, c) 950 °C, d) 1000 °C. Fase scura: σ. Tempo di permanenza in forno (τ) = 3 min.

C	Mn	Si	P	S	Cr	Ni	Mo	Cu	N	W	Fe
0.03 Max	1.00 Max	1.00 Max	0.0035 Max	0.015 Max	24.00-26.00	6.00-8.00	3.00-4.00	0.50-1.00	0.20-0.30	0.50-1.00	bal.

TAB. 1 ***Chemical composition (wt%) of UNS S32760 SDSS analysed.***
Composizione chimica nominale (wt%) dell'acciaio inossidabile superduplex UNS S32760 analizzato.

	800 °C	900 °C	950 °C	1000 °C
1 min		1.64 ± 0.3		
3 min	0.253 ± 0.1	12.771 ± 0.5	3.724 ± 0.8	
10 min	3.945 ± 0.9	23.332 ± 2.2	6.947 ± 1.8	0.467 ± 0.1
30 min		35.968 ± 3.0		
180 min	53.440 ± 4.9	41.716 ± 1.7	23.814 ± 1.8	1.024 ± 0.3
420 min	57.828 ± 3.1	49.357 ± 2.7	39.374 ± 2.4	4.805 ± 0.3

TAB. 2
Volume fraction (%) of sigma phase for isothermal treatments.
Frazione di volume (%) della fase sigma precipitata a temperatura costante.

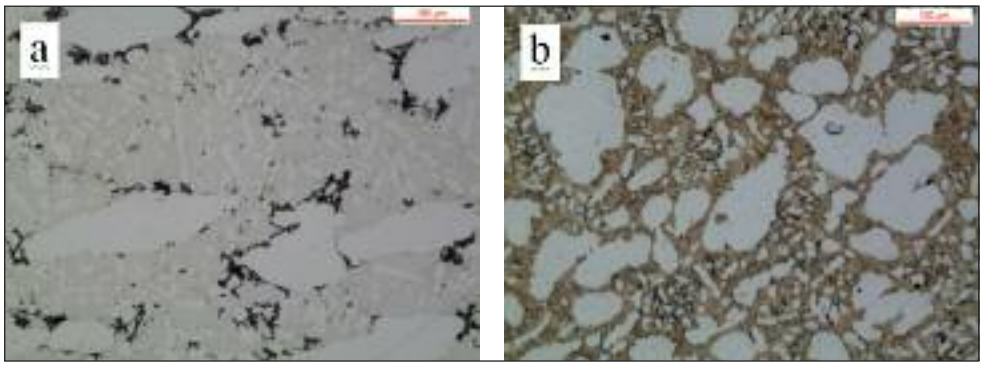

FIG. 3
Microstructure of the heat-treated material (continuous cooling) a) 0.19 °C/sec, b) 0.044 °C/s.
Microstrutture ottenute al variare della velocità di raffreddamento a) 0.19 °C/s b) 0.044 °C/s.

Mean cooling rate (°C/s)	% σ phase formed
4	0
0.19	4.171 ± 1.469
0.044	44.981 ± 4.911

TAB. 3 ***Volume fraction of sigma phase present in the microstructure at room temperature after anisothermal heat treatments.***
Frazione di volume della fase sigma a temperatura ambiente ottenute variando la velocità di raffreddamento.

untransformed matrix due to competitive growth of the fraction products, a direct collision of two advancing reaction products, or an exhaustion of nucleation sites.

$$\ln_{-}\ln|1-p|=n\ln t+\ln b \qquad (9)$$

The best correlation between the experimental and calculated sigma-phase evolution is obtained for c=1.9 (V_{max} is assumed constant with temperature and equal to 57%).
Since the experimental values of sigma phase proportions below 1 pct are associated with large inaccuracies, often of the same order as the measured value, a good agreement can be observed in Fig. 5. In this figure a comparison between the Avrami and the

T (°C)	800	900	950	1000
n	2.578	1.020	0.8161	0.651
b x 10^{-6} (s^{-1})	664.00	1060.07	118.94	0.64

TAB. 4 ***Obtained values of n and b coefficients by using the modified JMAK model.***
Valori dei coefficienti n e b del modello modificato di JMAK.

modified JMAK equation is also shown. It can be observed that at high temperatures (above 950 °C) the two models give similar results in agreement with the experimental values. It can be attributed both to a different mechanism of sigma phase precipitation at higher temperatures (if compared to the mechanism at lower temperatures) [27] and to a minor influence of the impingement factor on the precipitation model.
Numerical values of n and b coefficients obtained by means of the modified JMAK model are collected in Table 4.
In Fig. 6 both TTT and CCT diagrams representing 1 pct σ-phase are shown.
It can be observed a good correlation between experimental and analytical results. In particular, the model predicts a cooling rate, for the precipitation of about 4 pct σ phase, of 0.19 °C/s which is in good agreement with the experimental observations (Tab. 3).
Finally, due to the slow heating of the furnace, a correction fac-

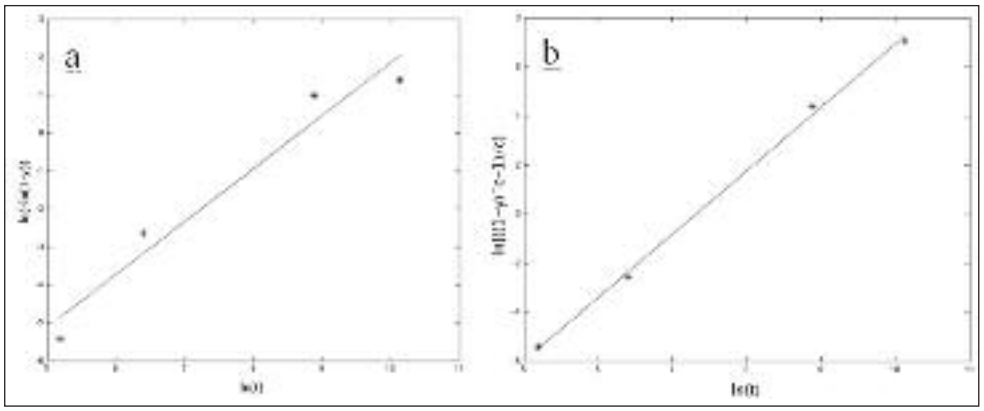

FIG. 4
Application of the classical Avrami model (a) and modified JMAK model to the -phase precipitation during aging at 800 °C.
Applicazione del modello classico di Avrami (a) e di quello modificato (JMAK) (b) alla precipitazione di fase sigma durante invecchiamento a 800 °C.

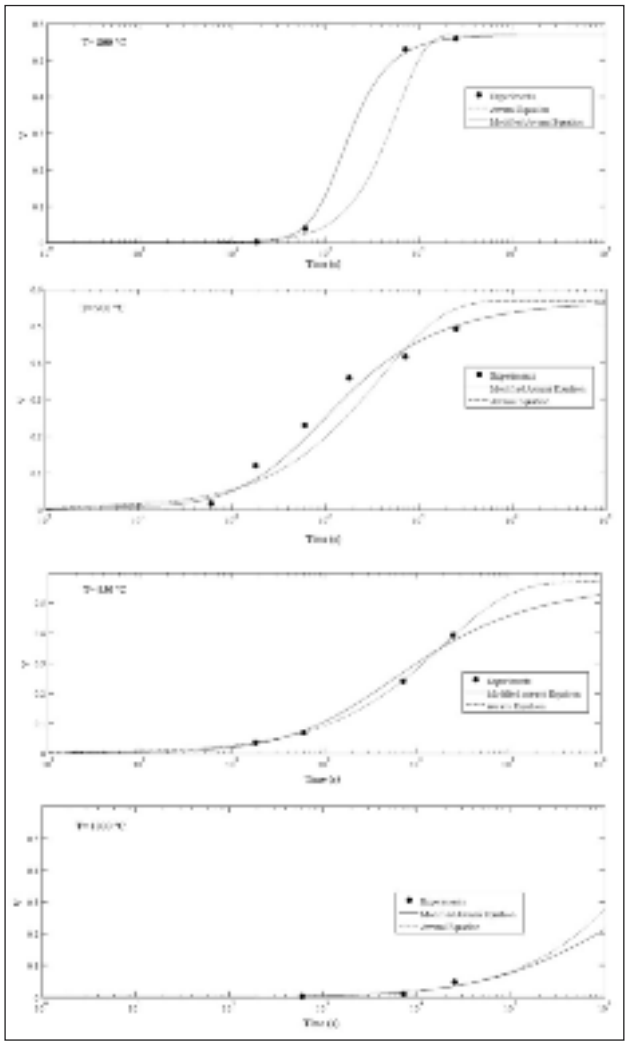

FIG. 5 ***Comparison between experimental and analytical results: isothermal -phase precipitation.***

Confronto fra i risultati analitici e sperimentali: precipitazione isoterma di fase sigma.

tor (R = 2000 s) was used in order to adjusting the parameters n and b. In order to support such observation, Wilson and Nilsson [22] found that such correction factor decreased as the heating rate increased.

CONCLUSIONS

In this work a semiempirical model was used for the characterization of σ-phase precipitation kinetics in UNS S32760 SDSS. Starting from isothermal heat treatments in the temperature range 800-1000 °C, the parameters of the modified JMAK equation have been obtained by interpolating analytical and experimental values at different times. In order to predict the CCT diagram, the additivity rule was assumed and calculated by means of a computer program written in Matlab® code. The flow chart for the computer program followed that developed in literature by Wilson and Nilsson. However, compared to this last work, the modified JMAK model was seen to better predict the σ-phase evolution for the analysed SDSS.

ACKNOWLEDGEMENTS

The authors gratefully acknowledge L. Giacomelli and M. Longin (Forgerossi S.p.A., Arsiero, VI, Italy) for the materials supply.

REFERENCES

[1] F. Bonollo, A Tiziani, P. Ferro: Duplex Stainless Steels. 1 st ed., Iris Alvarez_Armas, Susanne Degallaix-Moreuil, Wiley, Great Britain, 2009, pp. 141-155.
[2] R. Cervo, P. Ferro, A Tiziani: J. Mater. Sci., 2010 vol. 45, pp. 4369-4377.
[3] R. Cervo, P. Ferro, A Tiziani, F. Zucchi: J. Mater. Sci., 2010, vol. 45, pp. 4378-4389.
[4] F. Zucchi, G. Brunoro, F. Bonollo, A. Tiziani: La Metallurgia Italiana, 3 (1997), pp 21-26.
[5] F. Bonollo, A. Tiziani, P. Ferro: La Metallurgia Italiana, Vol 97 (2) (2005), pp. 27-38,
[6] P. Ferro, R. Cervo, B. Vianello, F. Bonollo: La Metallurgia Italiana, vol. 101 (10), (2009), pp. 55-62.
[7] H. Sieurin, R. Sandström: Mater. Sci. Eng. A, 2007, Vol. 444, pp. 271-276.
[8] Chi-Shang Huang, Chia-Chang Shih: Mater. Sci. Eng., 2005, Vol. 402, pp. 66-75.
[9] M.B. Cortie, E.M. Jackson: Metallurgical and Materials Transactions A, 1997, Vol. 28A(12), pp. 2477-2484
[10] A.F. Padilha, R.L Plaut: Duplex Stainless Steels. 1 st ed., Iris Alvarez_Armas, Susanne Degallaix-Moreuil, Wiley, Great Britain, 2009, pp. 115-139.
[11] M.R. El Koussy, I.S. El Mahallawi, W. Khalifa, M.M. Al Dawood, M. Bueckins: Mater.Sci. Technol., 2004, Vol. 20, pp. 375-381.
[12] Y.S. Ahn, J.P. Kang: Mater. Sci. Technol., 2000, Vol. 16, pp. 382-387.
[13] T.H. Chen, K.L. Weng, J.R. Yang: Mater. Sci. Eng. A, 2002, Vol. 338, pp. 259-270.
[14] J.-O. Nilsson, A. Wilson: Materials Science and Technology, 1993, Vol. 9(7), pp. 545-554
[15] H. Sieurin, R. Sandström: Eng. Fract. Mech., 2006, Vol. 73, pp. 377-390.
[16] A. Dhooge, E. Deleu: Weld. World, 1997, Vol. 39, pp. 47-52.
[17] Thermo-Calc®, STT (Foundation of Computational Thermodynamics, Stockholm, Sweden) and TCS (Thermo-Calc Software AB, Stockholm, Sweden). http://www.thermocalc.com
[18] X. Li, A. P. Miodownik, and N. Saunders: Materials Science and Technology, 2002, Vol. 18, pp. 861-867.
[19] Y. J. Kim, L. S. Chumbley and B. Gleeson: Journal of Materials En-

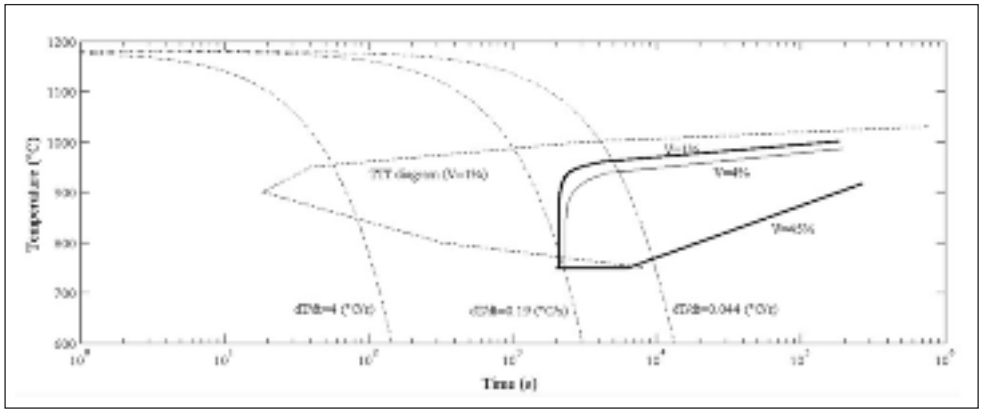

FIG. 6
Predicted TTT and CCT curves representing 1 pct , 4 pct and 45 pct σ phase.

Curve TTT e CCT predette dal modello.

gineering and Performance, 2008, Vol. 17(2), pp. 234-239.
[20] E. Sheil: Arch. Eisenhüttenwes., 1953, Vol. 12, pp 565-567.
[21] M. Lusk and H. J. Jou: Metallurgical and Materials Transactions A, 1997, Vol. 28A, pp. 287-291.
[22] A. Wilson and J.-O. Nilsson: Scand. J. Metall., 1996, Vol. 25, pp. 178-185.
[23] J.-O. Nilsson, P. Kangas, T. Karlsson and A. Wilson: Metallurgical and Materials Transactions A, 2000, Vol 31A, pp. 35-45.
[24] J.W. Elmer, T. A. Palmer, E. D. Specht: Metallurgical Transaction A, 2007, Vol. 38A, pp. 464-475.
[25] E.S. Lee, Y.G. Kim, Acta. Metall. Mater. 38 (9) (1990) 1667–1669.
[26] H.L. Lee and P.J. Moran, Metals and Materials. 4(5) (1998) 1085-1091.
[27] R. Magnabosco: Materials Research, 2009,Vol. 12, No 3, pp 321-327.

Abstract

Modello di precipitazione della fase sigma e sua applicazione all'acciaio inossidabile supeduplex UNS S32760

Parole chiave:
Acciaio inox, precipitazione, trattamenti termici, modellazione, produzione proprietà, qualità

È noto che la fase sigma, quando presente negli acciai inossidabili, ne riduce la resistenza a corrosione e la resilienza. La conoscenza dell'evoluzione microstrutturale indotta da un trattamento termico o processo di saldatura in questi materiali è perciò di fondamentale importanza al fine di ottimizzarne le prestazioni. Per questa ragione sono stati sviluppati diversi modelli di precipitazione delle fasi secondarie in funzione della temperatura e della velocità di raffreddamento, sia di tipo analitico che semi-empirico, atti a migliorare la progettazione dei trattamenti termici e dei processi di saldatura. Nonostante i modelli analitici offrano delle equazioni di evoluzione in forma chiusa, i diversi parametri di cui essi necessitano, sono spesso difficilmente reperibili o poco affidabili [23,24]. Al contrario, i modelli semi-empirici, pur necessitando di una campagna di dati sperimentali per la loro calibrazione, hanno il vantaggio di offrire risultati molto più affidabili.
Sulla base del lavoro pionieristico di Wilson e Nilsson [22], viene proposto in questo articolo un modello semi-empirico di evoluzione della fase sigma. Rispetto al precedente lavoro [22], al fine di considerare alcuni effetti locali (come la riduzione del contenuto di soluto nella matrice non ancora trasformata e causato dalla crescita competitiva dei precipitati, la diretta collisione di due prodotti di reazione o un esaurimento dei siti di nucleazione), il modello fa riferimento all'equazione modificata di Johnson–Mehl–Avrami-Kolmorgorov (JMAK) [25] che contiene un ulteriore parametro chiamato "impingement factor". La calibrazione del modello viene effettuata mediante una campagna di prove sperimentali a temperatura costante e l'evoluzione della fase secondaria in funzione della velocità di raffreddamento viene dedotta mediante la regola dell'additività (Eq. (1)). Il modello proposto, applicato all'acciaio inossidabile superduplex UNS S32760, ha fornito risultati in buon accordo con i valori sperimentali (Figura 6), evidenziandone la maggiore accuratezza rispetto al modello classico di Avrami (Figure 4 e 5).